ORIGINAL ARTICLE

Cartilage imaging of a rabbit knee using dual-energy X-ray microscopy and 1.0 T and 9.4 T magnetic resonance imaging

Ying Zhu, Sarah L. Manske, Steven K. Boyd*

McCaig Institute for Bone and Joint Health and Department of Radiology, Cumming School of Medicine, University of Calgary, Alberta, Canada

Summary *Background/Objective:* Osteoarthritis is a common chronic disease of the joints characterised by the degeneration of articular cartilages and subchondral bone. The most common diagnostic imaging used clinically is X-ray; however, it cannot directly image cartilage. Magnetic resonance imaging (MRI) is well suited for cartilage imaging, but it requires costly and lengthy scans. For preclinical work, microcomputed tomography provides high spatial resolution and contrast for bone, however, its standard application is not well suited for cartilage imaging.
Methods: We performed a preliminary investigation into the use of dual-energy X-ray microscopy (XRM) for cartilage imaging and analysis of a rabbit knee, and compared it to the MRI results from 9.4 T and 1.0 T small-animal scanners.
Results: The XRM images offer a higher image resolution ($\sim$25 μm nominal isotropic resolution) compared with the MRI (50—86 μm in plane, and 250 μm slice thickness). The cartilage-thickness measurements using the dual-energy XRM are on average 3.8% (femur) and 5.1% (tibia) thicker estimates than the 9.4 T MRI results. The cartilage-thickness measurements using the 1.0 T MRI are on average 10.9% (femur) and 2.3% (tibia) thinner estimates than the 9.4 T MRI results.
Conclusion: Our results suggest that the dual-energy XRM for articular-cartilage analysis is feasible and comparable to the MRI. This technology will provide good support for high-resolution animal-osteoarthritis studies, and in the future, it may be possible to apply dual energy in a clinical setting.

* Corresponding author. McCaig Institute for Bone and Joint Health, University of Calgary, Room HRIC 3AC64, 3280 Hospital Drive NW, Calgary, Alberta, T2N 4Z6, Canada.
    E-mail address: skboyd@ucalgary.ca (S.K. Boyd).

Introduction

Bone and joint diseases are leading causes of disability worldwide. Osteoarthritis (OA) is the most common chronic disease of the joints resulting in pain, stiffness, and disability. OA affected 13.9% of adults (25+ years old) and 33.6% of elders (65+ years old) in the United States in 2005 [1]. Particularly, knee OA affects 37.4% of elders (60+ years old) in the United States during 1991−1994, and it is a major cause of mobility impairment [2]. The Canadian OA healthcare expenditure is estimated $27.5 billion in 2010, and projected to rise to $1455.5 billion in 2040 [3]. Currently, there is no cure for OA. Characterised by degeneration of articular cartilage and changes in subchondral bone and other soft-tissue structures, anatomic OA changes may occur earlier than OA symptoms [4,5]. The accurate and sensitive imaging of articular cartilage and subchondral bone is a likely key to an early diagnosis, and for tracking the disease progression and assessing treatments for OA.

There are currently no three-dimensional (3D) techniques available to image cartilage clinically that are based on using X-rays. Radiography is routinely used for assessing joint-space loss, subchondral sclerosis, subchondral cyst formation, and marginal osteophyte formation in OA, but not the articular cartilage itself [6], and thus, limits the sensitivity to make early diagnoses of OA. Magnetic resonance imaging (MRI) is the predominant imaging modality for visualising soft tissue, and there is a significant body of work that has been published using clinical or preclinical, low-field or high-field MRI for quantitative articular-cartilage measurements (volume, thickness, and even composition) [7−13] with validation using histology [14]. MRI is well suited for cartilage imaging and results in no radiation exposure, but it requires costly and lengthy scans at a limited image resolution relative to the cartilage thickness, is not well suited for bones, and is challenging for patients with metallic implants. There is a need for complementary or alternative diagnostic-imaging methods for early OA.

Both clinical [15] and preclinical [16] microcomputed tomography (CT) can provide high spatial resolution and contrast for bones, and are relatively fast and inexpensive; however, in their standard application, they are not well suited for cartilage imaging. Contrast agents can be used to enhance the visualisation of articular cartilage in preclinical settings [17], but ideally are avoided. There is a need for new quantitative-analysis methods to be developed for X-ray imaging of articular cartilage, and doing so would lead to a promising diagnostic tool for early OA detection.

This study provided a preliminary investigation into using a novel dual-energy imaging technology in X-ray microscopy (XRM) for knee-cartilage analysis in a preclinical small-animal model. XRM is distinct from the traditional micro-CT because it combines both geometric magnification and optical objectives of microscopy to achieve higher (submicrometer) spatial resolution at a relatively longer (~50 mm) working distance. The enabling technology of dual-energy imaging for soft tissues is based on different tissue responses on X-ray attenuation to energy-spectrum changes. Specifically, cartilage morphology and thickness measurements were analysed in a normal knee joint of a rabbit model using a 9.4 T small-animal MRI scanner (Magnex Scientific, Yarnton, UK) as a gold standard for XRM measurements. A dual-energy imaging analysis was performed on the same sample using the latest-generation preclinical XRM scanner (Versa 520; Carl Zeiss X-ray Microscopy, Pleasanton, CA, USA). In comparison, the imaging capacity of a newly installed 1.0 T compact MRI desktop system (ICON M2; Bruker, Billerica, MA, USA) was also explored, as it offers similar advantages as XRM due to it being a desktop technology, albeit at a lower resolution. Our aim was to explore the utility of dual-energy imaging for cartilage assessment. The advantage of XRM is that it can simultaneously capture subchondral-bone measurements (density and microstructure) along with the articular cartilage. We hope that, by developing dual-energy procedures in a preclinical model, we can eventually translate our findings to clinical applications with clinical CT scanners in the future. The analysis of articular cartilage using X-ray techniques, both preclinically and clinically, will be valuable tools for translational research in the area of OA.

Materials and methods

Specimens

One knee joint (left knee) was excised from a 7-month-old, normal rabbit immediately after euthanasia at the animal centre following the approved University of Calgary ethics protocol #AC11-0039. The fresh knee joint was preserved in 10% neutral-buffered formalin. Before the imaging experiments, the distal femur and proximal tibia were surgically separated while keeping the articular cartilage intact.

9.4 T MRI

The rabbit femur and tibia were immersed in Fluorinert FC-770 buffer (3M Electronics, St. Paul, MN, USA) and sealed in centrifuge tubes to maintain sample moisture without introducing signal to the MRI. The 9.4 T MRI scanner (Figure 1D) is equipped with a 21-cm horizontal bore, a Bruker gradient (BGA12S, 720 mT/m), and a Bruker console (AVANCE II, running the ParaVision software). The sample was secured in a birdcage radio-frequency coil (35-mm-diameter quadrature volume coil) and scout scanned transversely, coronally, and sagittally to cover the full size of each bone. The data collection was performed on the sagittal plane (Figure 1A), which would provide a precise measurement of the articular cartilage. To achieve high vibration stability and high pixel resolution (50 μm) in the sagittal plane, 16 scans of five slices each (250 μm slice thickness) were sequentially performed back to back using two-dimensional (2D) gradient-echo fast-low-angle-shot sequence (6.034-millisecond echo time, 125-millisecond repetition time, and 30° flip angle). This sequence was optimal for the visualisation of the articular cartilage in our settings. With six images averaged for each slice, the total image set of 512 pixels × 512 pixels × 80 pixels covering 2.56 cm × 2.56 cm × 2.00 cm, a full size of the sample, took 1 hour and 42 minutes of scan time for each of the femur and tibia.
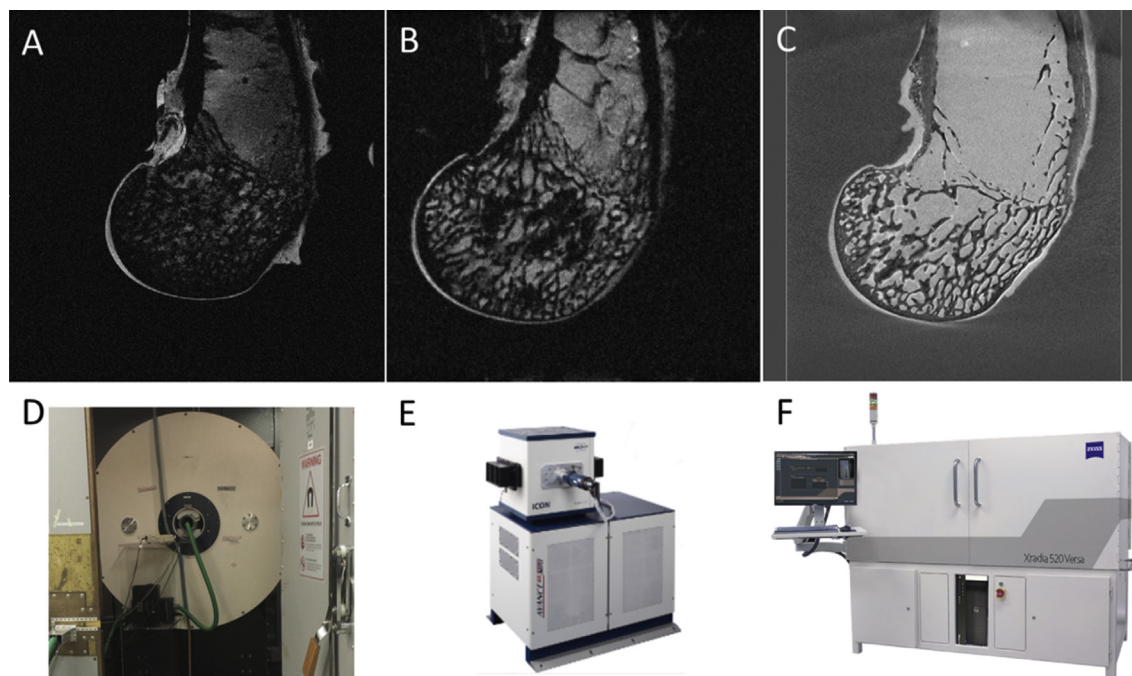
Figure 1 (A—C) Image data of a rabbit femur and (D—F) their scanners. (A) Image of a raw slice in the sagittal plane after rotation, from the (D) 9.4 T magnetic-resonance-imaging scanner. (B) Image of a raw slice in the sagittal plane after averaging, from the (E) 1.0 T magnetic-resonance-imaging scanner. (C) Image of a contrast-combined slice from high- and low-energy images after orientation in the sagittal plane, from the (F) dual-energy X-ray-microscopy scanner.

1.0 T MRI

The rabbit femur and tibia were wrapped with water-soaked paper tissue around the bone shaft, sealed by a plastic wrap, and secured in the chamber of the device. The 1.0 T MRI scanner (Figure 1E) is equipped with a horizontal bore, a Bruker gradient (450 mT/m), and a Bruker console (digital radio-frequency AVANCE III, running the ParaVision software). The sample was scout scanned transversely, coronally, and sagittally to cover the full size of each bone, and the data collection was performed on the sagittal plane (Figure 1B). To achieve magnetic-field stability and an optimal pixel resolution in the sagittal plane (80.1 μm for femur and 85.9 μm for tibia), four scans of 20 slices each (250 μm slice thickness) were sequentially performed back to back using a 2D gradient-echo fast-low-angle-shot sequence (8-millisecond echo time, 1000-millisecond repetition time, 80° flip angle at 15 kHz main bandwidth, and 1.34 resolution encoding partial Fourier transform and 63 partial Fourier transform overscans). To achieve a high signal-to-noise ratio, two sets of full sample scan were performed with 40 images averaged for each slice of each scan. The total image set of 256 pixels × 256 pixels × 80 pixels covering 2.05 cm × 2.05 cm × 2.00 cm (femur) or 2.20 cm × 2.20 cm × 2.00 cm (tibia), a full size of the sample, took 22 hours and 45 minutes for each of the femur and tibia.

Dual-energy XRM

The rabbit femur and tibia were sealed in centrifuge tubes with phosphate-buffered saline solution soaking the bone shaft. The XRM scanner (Figure 1F) is a preclinical sample-rotating system providing large working distance, adjustable energy range, switchable optical objectives, and automatic X-ray filter change. Both low-energy (40 kVp voltage, 3 W power, and no extra filter) and high-energy (150 kVp voltage, 10 W power with a custom filter) XRM scans were performed on the same sample sequentially using the 0.4× objective, which is sensitive to high-energy photons. To achieve a high signal-to-noise ratio, 2501 projections were collected per rotation with each single projection exposure time of 3 seconds for low energy and 1.5 seconds for high energy. The two sets of raw data of 1004 pixels × 1024 pixels × 1004 pixels with a nominal isotropic resolution of 22.3 μm (femur) and 25.1 μm (tibia) took approximately 6 hours of scanning time for each of the femur and tibia.

Data analysis

The MRI data sets were imported into the Fiji image-processing software [18] (http://fiji.sc/Fiji; National Institutes of Health, Bethesda, MD, USA) and organised into 3D data sets. For repeated scans from the 1.0 T MRI data, 2D rigid image registration was performed using a Fiji plugin (Register Virtual Stack Slices [19]) and a custom developed script (Jython version 2.7, www.jython.org [20], Python Software Foundation) for automatic image registration and image averaging for the whole data sets.

Both high- and low-energy XRM data were loaded into software for image registration and dual-energy analysis (Dual-Scan Contrast Visualizer [21]; Carl Zeiss X-ray Microscopy). In its intensity 2D histogram (Figure 2), which tends
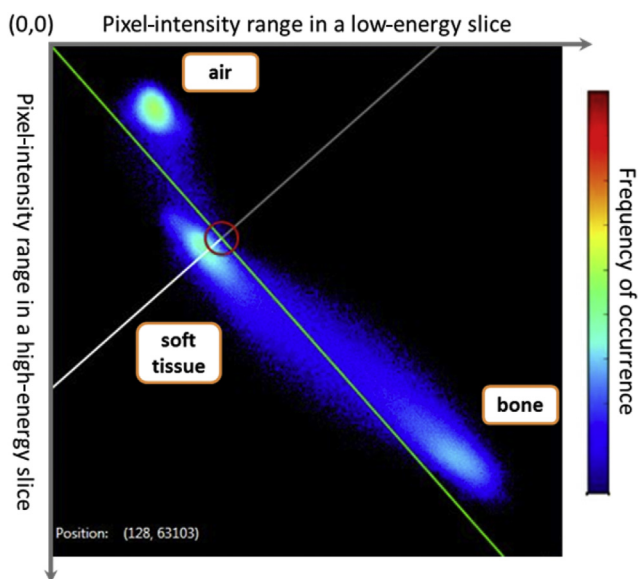
Figure 2 Intensity two-dimensional histogram of a slice in the Dual-Scan Contrast Visualizer software. The coordinates of a point are the pixel-intensity values in low- and high-energy images, and the colour represents the frequency of the occurrence of the intensity combinations. The green line segments the image to enhance the pixels in the white-line region and to weaken the pixels in the grey-line region.

to converge pixels of similar material and density due to similar intensity variation, the soft-tissue cluster that included the cartilage was separated (green line) from the bone cluster and air cluster, and was enhanced in the final data set. Because the dual-energy XRM data were collected with slices in the transversal plane, the data were transformed to sagittal-plane slices (Figure 1C) to facilitate segmentation of the articular cartilage.

The MRI data and the dual-energy XRM data were imported into the image-processing-language image-analysis software (SCANCO Medical, Brüttisellen, Switzerland) for semi-automated cartilage segmentation performed in the sagittal-plane slices using the snakes algorithm [22] (setting inner to 500 and outer to 155 for the MRI, and 100 for the dual-energy data). For the MRI data, the nonisotropic 3D data set was scaled to the isotropic 3D data set for the cartilage analysis.

The thickness of the cartilage after segmentation was calculated based on a distance-transformation method over the articular surfaces [23]. The visualisation of the thickness maps using a pseudocolour scale enabled the qualitative comparison of cartilage morphology and thickness distribution amongst the data sets produced by the three imaging modalities, and a quantitative analysis was performed on the mean value and standard deviation of the total cartilage thickness, as well as the total volume of the measured cartilage tissue.

Results

The cartilage-thickness maps of the rabbit femur (Figure 3) and tibia (Figure 4) clearly exhibited a high consistency in cartilage morphology amongst the three imaging modalities, and a greater image resolution of the dual-energy XRM (22.3 μm and 25.1 μm nominal isotropic voxel size for the femur and tibia, respectively) compared with the MRI (50.0 μm, 80.1 μm, and 85.9 μm in-plane, and 250 μm slice thickness).

To test the reproducibility of the dual-energy XRM analysis, the same rabbit femur was repositioned in the centrifuge tube, underwent the same scanning and post-processing procedures, and produced cartilage-thickness maps, as shown in Figure 5A. Their difference map of cartilage thickness (Figure 5B) from the original scan (Figure 3C) was obtained after performing 3D imaging registration using the image-processing-language image-analysis software (SCANCO Medical). The voxel of exact match (0-mm-thickness difference) is shown in green–yellow colour, as noted in the colour bar. The average thickness difference is 1.0 μm with a standard deviation of 123.2 μm.

A summary of the quantitative data (Table 1) shows that the mean cartilage-thickness measurements using the dual-energy XRM are 329-μm thick at the femur and 509-μm thick at the tibia. These results are 3.8% (femur) and 5.1% (tibia) thicker than the 9.4 T MRI results. The absolute thickness differences of 12.2 μm (femur) and 24.9 μm (tibia) are no more than one pixel size from the XRM. The mean cartilage-thickness measurements using the 1.0 T MRI are 10.9% (femur) and 2.3% (tibia) thinner than the 9.4 T MRI results. The absolute thickness differences of 34.6 μm (femur) and 11.2 μm (tibia) are less than one pixel size from the 1.0 T MRI.

Discussion

We have explored three imaging modalities aimed at measuring articular cartilage in a rabbit knee. Notably, the dual-energy XRM data were able to isolate the cartilage soft tissue from the femur and tibia scans, and provided comparable quantitative measurements to the MRI.

There are many factors that can influence our cartilage-thickness measurements. The differences between the 9.4 T MRI and the dual-energy XRM come in part from the challenge of selecting an appropriate threshold to enable the cartilage segmentation. The selection of a threshold was done qualitatively for this preliminary study; however, a more rigorous approach will need to be developed for the future. A possible option is to use the MRI as a gold standard against which an appropriate threshold can be selected for the dual-energy XRM based on the optimal matching of thickness maps. Another challenge in our study is that the MRI inert buffer Fluorinert FC-770 adds no signal to the MRI, whereas extra surface moisture of the cartilage can be picked up as soft tissue in the XRM measurements. It was challenging to keep the surface moisture level the same for the three specimen wrappings in the three systems, particularly due to the differences in scan time. For example, the scan time of the 1.0 T MRI was >22 hours, whereas the scan time of the 9.4 T MRI was <2 hours. In short, although we recognise that thickness differences are affected by many factors for the three imaging modalities explored, the overall level of agreement was good.
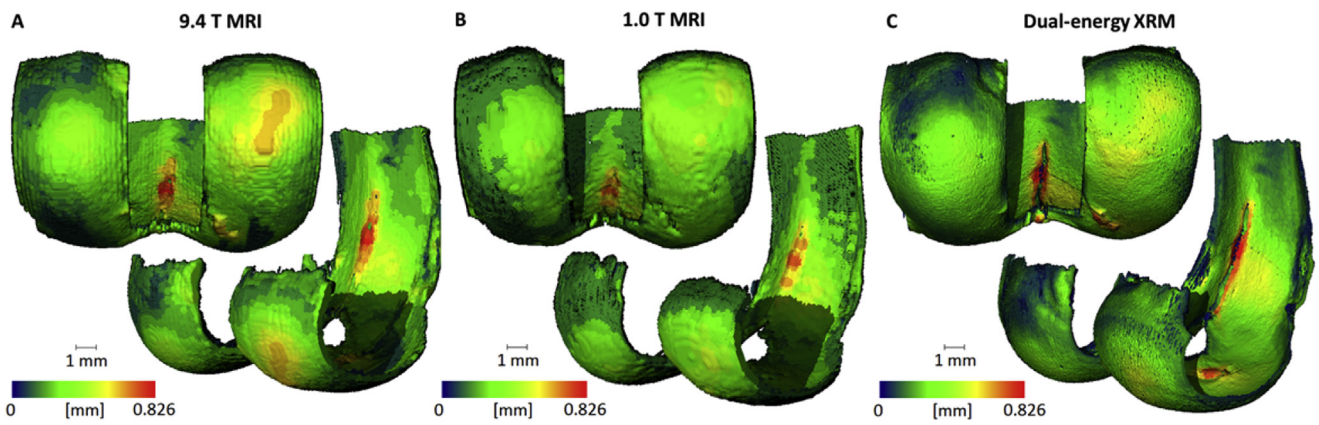
Figure 3 Cartilage morphology and thickness maps (colour bar) of a rabbit femur in two views by (A) 9.4 T magnetic-resonance imaging, (B) 1.0 T magnetic-resonance imaging, and (C) dual-energy X-ray-microscopy analysis. MRI = magnetic-resonance imaging; XRM = X-ray microscopy.

The repeated measure of the femur showed that the dual-energy XRM provided a reproducible analysis, and the agreement for the cartilage-thickness mean is 99%, including the effects of the semiautomated cartilage-segmentation process, and thus, the different total cartilage volume.

The desktop 1.0 T MRI scanner provided comparable measurements to those performed on the 9.4 T MRI, albeit with a much longer scan time. Although the 9.4 T MRI is still preferred due to its superior image resolution and shorter scan time, it is encouraging that a compact desktop system could provide a good estimation of cartilage thickness. The 1.0 T MRI appears to be a useful technology for preclinical imaging and a reasonable alternative when a 9.4 T MRI is not available.

Besides radiation exposure, one of the limitations of the dual-energy XRM is that it is not straightforward to distinguish between soft tissues, including cartilage, meniscus, and ligament. These tissues' X-ray absorption coefficients are close, and adjacent tissues of similar types are not evident in the 2D histogram plot, particularly if the volume of that tissue type in an image slice is not substantial. This might be solved by referring to a histogram combining the total volume rather than by slice, and will be explored in the future. We showed the dual-energy XRM provided a good estimate of cartilage thickness, and we intend to explore other features of our XRM scanner, particularly the use of phase-contrast imaging that would distinguish boundaries of different soft-tissue types, such as cartilage, meniscus, and synovial fluid. This potentially would further extend our abilities for preclinical measurement of articular cartilage.

A limitation of this study was that the knee joint was not assessed intact, but instead, the femur and tibia were
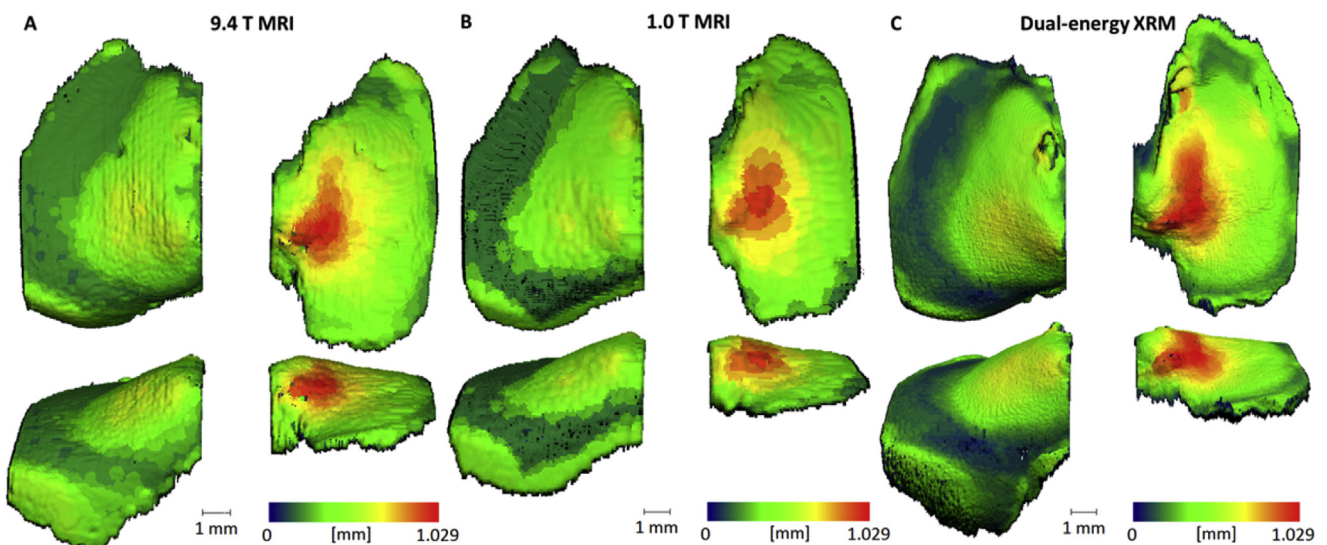

Figure 4 Cartilage morphology and thickness maps (colour bar) of a rabbit tibia in two views by (A) 9.4 T magnetic-resonance imaging, (B) 1.0 T magnetic-resonance imaging, and (C) dual-energy X-ray-microscopy analysis. MRI = magnetic-resonance imaging; XRM = X-ray microscopy.
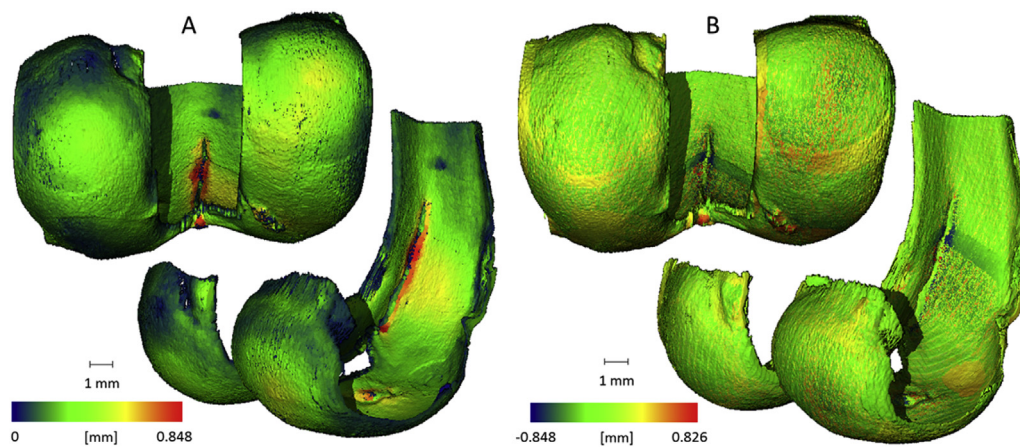
Figure 5 A reproducibility study of the same rabbit femur by the dual-energy X-ray-microscopy analysis. (A) The image is the cartilage morphology and thickness map (colour bar) of the validation scan in two views. (B) The image is the difference map of cartilage thickness between the original scan (Figure 3C) and the (A) validation scan after image registration.

Table 1 Quantitative cartilage-analysis summary by three imaging modalities.

Cartilage-analysis	Rabbit femur			Rabbit tibia		
Imaging modalities	9.4 T MRI	1.0 T MRI	Dual-energy XRM	9.4 T MRI	1.0 T MRI	Dual-energy XRM
In-plane pixel resolution (μm)	50.0	80.1	22.3	22.3	50.0	85.9	25.1
Slice thickness (μm)	250.0	250.0	22.3	22.3	250.0	250.0	25.1
Cartilage-thickness mean (μm)	316.4	281.8	326.7	330.4	483.9	472.7	508.8
Cartilage-thickness standard deviation (μm)	142.6	115.1	155.5	159.2	201.7	202.3	236.1
Total cartilage volume (mm^3)	86.0	80.4	94.1	93.7	63.9	64.4	66.5
Cartilage-thickness mean differences (%)	0	−10.9	3.3	4.4	0	−2.3	5.1
Cartilage-thickness mean differences (μm)	0	−34.6	10.3	14.0	0	−11.2	24.9

MRI = magnetic-resonance imaging; XRM = X-ray microscopy.

excised from the joint. The moisture surrounding the articular surfaces in our scanning protocol somewhat simulates the intact joint in terms of the challenge of measuring cartilage thickness, however, further studies are needed using intact joints. In addition, we would like to perform these comparisons on a variety of joints, and test the limits of preclinical imaging on different animal models from small (e.g., mouse) to large (e.g., dog).

The major advantage of using the dual-energy XRM is that it is ideal for measuring hard tissue, such as subchondral bone, as well as soft tissue, such as cartilage, all simultaneously with the same system. This will lead to robust and reproducible results on the dual-energy XRM, which we will validate on a range of sample sizes in the near future. We have recently purchased a dual-energy clinical CT scanner that we intend to use to explore the use of cartilage measurements in a clinical setting. Having a range of preclinical to clinical methodologies for cartilage-thickness measurements will be useful in the field of OA research in the future.

Conflicts of interest

All contributing authors declare no conflicts of interest.

References

[1] Lawrence RC, Felson DT, Helmick CG, Arnold LM, Choi H, Deyo RA, et al. Estimates of the prevalence of arthritis and other rheumatic conditions in the United States. Part II. Arthritis Rheum 2008;58:26—35.
[2] Dillon CF, Rasch EK, Gu Q, Hirsch R. Prevalence of knee osteoarthritis in the United States: arthritis data from the

Third National Health and Nutrition Examination Survey 1991—1994. J Rheumatol 2006;33:2271—9.

[3] Bombardier C, Hawker G, Mosher D. The impact of arthritis in Canada: today and the next 30 years. Arthritis Alliance of Canada; 2011. p. 1—51.

[4] Hannan MT, Felson DT, Pincus T. Analysis of the discordance between radiographic changes and knee pain in osteoarthritis of the knee. J Rheumatol 2000;27:1513—7.

[5] Hunter DJ, Guermazi A, Roemer F, Zhang Y, Neogi T. Structural correlates of pain in joints with osteoarthritis. Osteoarthritis Cartilage 2013;21:1170—8.

[6] Jacobson JA, Girish G, Jiang Y, Sabb BJ. Radiographic evaluation of arthritis: degenerative joint disease and variations. Radiology 2008;248:737—47.

[7] Eckstein F, Burstein D, Link TM. Quantitative MRI of cartilage and bone: degenerative changes in osteoarthritis. NMR Biomed 2006;19:822—54.

[8] Wang YX. In vivo magnetic resonance imaging of animal models of knee osteoarthritis. Lab Anim 2008;42:246—64.

[9] Faure P, Doan BT, Beloeil JC. In vivo high resolution three-dimensional MRI studies of rat joints at 7 T. NMR Biomed 2003;16:484—93.

[10] Hardy PA, Newmark R, Liu YM, Meier D, Norris S, Piraino DW, et al. The influence of the resolution and contrast on measuring the articular cartilage volume in magnetic resonance images. Magn Reson Imaging 2000;18:965—72.

[11] Laurent D, Wasvary J, O'Byrne E, Rudin M. In vivo qualitative assessments of articular cartilage in the rabbit knee with high-resolution MRI at 3T. Magn Reson Med 2003;50:541—9.

[12] Wang YX, Griffith JF, Ahuja AT. Non-invasive MRI assessment of the articular cartilage in clinical studies and experimental settings. World J Radiol 2010;2:44—54.

[13] Link TM, Majumdar S, Peterfy C, Daldrup HE, Uffmann M, Dowling C, et al. High resolution MRI of small joints: impact of spatial resolution on diagnostic performance and SNR. Magn Reson Imaging 1998;16:147—55.

[14] Tessier JJ, Bowyer J, Brownrigg NJ, Peers IS, Westwood FR, Path FRC, et al. Characterisation of the guinea pig model of osteoarthritis by in vivo three-dimensional magnetic resonance imaging. Osteoarthritis Cartilage 2003;11:845—53.

[15] Boyd SK, Manske SL, Burt LA, Jorgenson B, Zhu Y, Hilderbrandt EM, et al. High resolution imaging of bone microarchitecture in the human appendicular skeleton. J Orthop Transl 2014;2:201—2.

[16] Manske SL, Good CA, Zernicke RF, Boyd SK. High-frequency, low-magnitude vibration does not prevent bone loss resulting from muscle disuse in mice following Botulinum toxin injection. PLoS One 2012;7:1—11. e36486.

[17] Silvast TS, Kokkonen HT, Jurvelin JS, Quinn TM, Nieminen MT, Toyras J. Diffusion and near-equilibrium distribution of MRI and CT contrast agents in articular cartilage. Phys Med Biol 2009;54:6823—36.

[18] Schindelin J, Arganda-Carreras I, Frise E, Kaynig V, Longair M, Pietzsch T, et al. Fiji: an open-source platform for biological-image analysis. Nat Methods 2012;9:676—82.

[19] Cardona A, Arganda-Carreras I, Saalfeld S. Register virtual stack slices (Fiji), version 2.0.0, Free Software Foundation Inc, 2014. Available at: http://fiji.sc/Register_Virtual_Stack_Slices. [accessed 01.03.15].

[20] Chekanov SV. Scientific data analysis using Jython scripting and Java. London: Springer—Verlag; 2010.

[21] DSCoVer — Dual Scan Contrast Visualizer, version 10.7.2936, Carl Zeiss X-ray Microscopy, Pleasanton CA USA, 2014. Available at: http://www.zeiss.com/microscopy/en_us/products/x-ray-microscopy/zeiss-xradia-520-versa.html. [accessed 01.03.15].

[22] Buie HR, Campbell GM, Klinck RJ, MacNeil JA, Boyd SK. Automatic segmentation of cortical and trabecular compartments based on a dual threshold technique for in vivo micro-CT bone analysis. Bone 2007;41:505—15.

[23] Laib A, Rüegsegger P. Comparison of structure extraction methods for in vivo trabecular bone measurements. Comput Med Imaging Graph 1999;23:69—74.